COMMUNICATION

Functionalized 3D Architected Materials via Thiol-Michael Addition and Two-Photon Lithography

Daryl W. Yee, Michael D. Schulz, Robert H. Grubbs, and Julia R. Greer**

In recent years, two-photon lithography (TPL) has emerged as a powerful tool to create complex, small-scale 3D materials.[1–6] By focusing a femtosecond laser into a negative-tone photoresist, polymerization can be locally induced within the focal region of the beam. Rastering the laser focus throughout the photoresist in three dimensions then enables the creation of polymer structures with virtually any geometry.[7–9] This architectural versatility renders these 3D polymer structures useful for many technological applications, including drug delivery,[10–12] tissue engineering,[13–15] micro-/nano-optics,[16,17] and photonics.[18,19]

To further expand the application of these 3D structures, it is not only important to precisely engineer the structure and architecture of the material, it is also necessary to have control over the chemical functionality on the surface and/or in the volume of these 3D structures. As a result of this, the fabrication of functional 3D structures has been an area of active research in recent years. One approach often taken is the addition of functional nanoparticles or its precursors into the photoresist, which then get incorporated into the structure during photopolymerization. Structures with magnetic,[20–22] luminescence,[23–25] and electrical[26–30] properties can be fabricated in this fashion. While simple, a common drawback with this method is that agglomeration of these particles interferes with the ability of the laser to penetrate into the resin, limiting the doping concentration of these nanoparticles.[24] Another approach has been to postfunctionalize the structure by reacting the residual unreacted polymerizing groups on the surface with the appropriate molecules. For example, epoxide moieties can be ring-opened to form hydroxyl groups that can be used for further reaction,[31,32] acrylates groups can undergo Michael addition with nucleophiles[33] or free-radical addition with other acrylate-terminated molecules,[34] and thiols can participate in thiol-Michael addition reactions.[35,36] This method allows for some flexibility in tailoring the functionality of the structure, however, as a significant number of polymerizing groups are consumed during the polymerization process, there are relatively few unreacted groups for postfunctionalization. Quick et al. showed that for a thiol–ene photoresin, the density of unreacted thiol groups available for postfunctionalization was ≈200 molecules μm^{-2}.[35]

D. W. Yee, Prof. J. R. Greer
Division of Engineering and Applied Science
California Institute of Technology
CA 91125, USA
E-mail: daryl@caltech.edu; jrgreer@caltech.edu
Dr. M. D. Schulz, Prof. R. H. Grubbs
Division of Chemistry and Chemical Engineering
California Institute of Technology
CA 91125, USA

DOI: 10.1002/adma.201605293

A more modern approach has been to synthesize monomers with the functional groups of interest. By carefully designing the monomers such that the desired functional groups are not consumed during the polymerization process, structures with unique properties such as photoreactive surfaces,[37–39] intrinsic chemical sensing,[40] chemical resistance,[41] bioactivity,[42,43] and biodegradability[44,45] can be fabricated. Since the functional groups are directly installed onto the monomer, they should exhibit a higher surface density of functional groups. Unfortunately, these functional monomers are often difficult to synthesize, requiring a controlled atmosphere and/or a complex, multistep synthesis.

Here, we present a facile method of fabricating functional 3D structures by prefunctionalizing a multifunctional acrylate monomer via the thiol-Michael addition reaction prior to TPL. To demonstrate the versatility of this method, we used a variety of thiols to produce acrylates with different functionalities. The functionalized acrylates were then mixed with a two-photon photoinitiator in an appropriate solvent and used to fabricate 3D structures via TPL. Several different 3D geometries were fabricated; their morphologies were analyzed via scanning electron microscopy (SEM), and the presence of functional groups on the surfaces was verified using a combination of energy-dispersive X-ray spectroscopy (EDS) and X-ray photoelectron spectroscopy (XPS). Contact angle measurements were used to highlight the changes associated with surface functionalization and fluorescence microscopy to demonstrate the potential of some of the functional photoresists in subsequent postfunctionalization reactions.

The development of the new functional photoresists was guided by the following design criteria: i) ease of preparation, ii) ability to functionalize with a wide variety of functional groups, iii) a high degree of functionality, iv) compatibility with current TPL systems, and v) long shelf-lives. To ensure compatibility with TPL systems, we based our approach on the widely used pentaerythritol tetraacrylate (PETTA) system with minimal modifications. **Figure 1**a shows that the thiol-Michael addition reaction of a thiol with PETTA enabled the attachment of the desired functionality directly onto the monomer while maintaining a degree of acrylate functionality equivalent to pentaerythritol triacrylate. Thiol-Michael addition offers several advantages: i) the reaction is simple to set up and is insensitive to air and moisture, requiring just the thiol, olefin, and an amine as a catalyst; ii) the reaction is quantitative in most cases; iii) a wide variety of functional thiols are commercially available; and iv) no by-products are produced, which enables immediate use of the new monomer after synthesis without requiring additional purification.

The functionalized acrylate was synthesized by reacting the multifunctional acrylate, PETTA, with a thiol via the

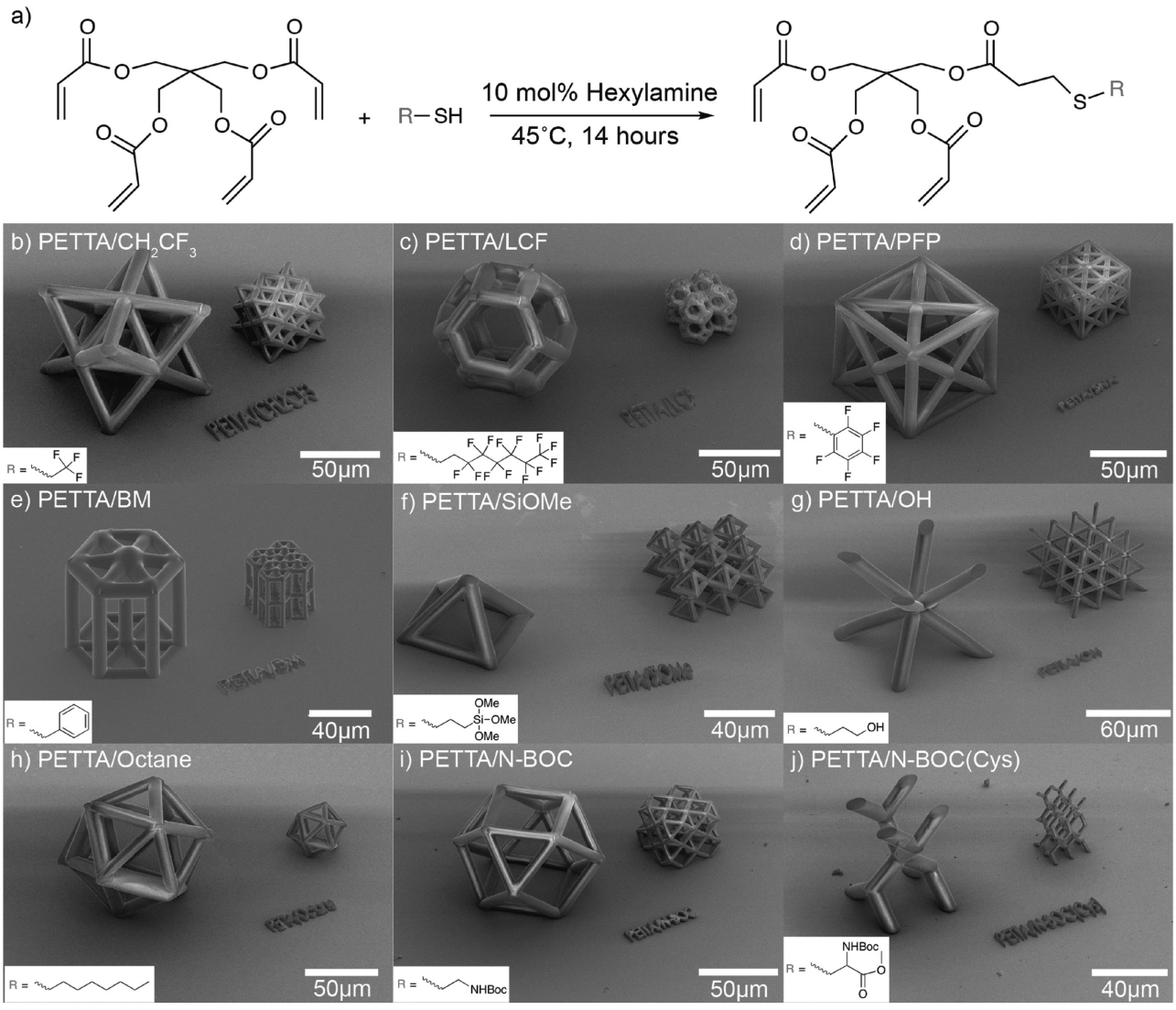

Figure 1. a) Chemical structure of the functional monomers synthesized by reacting pentaerythritol tetraacrylate with a thiol via the thiol-Michael reaction. Representative product shown. SEM images of the architected materials written with b) PETTA/CH_2CF_3, c) PETTA/LCF, d) PETTA/PFP, e) PETTA/BM, f) PETTA/SiOMe, g) PETTA/OH, h) PETTA/octane, i) PETTA/N-BOC, and j) PETTA/N-BOC(Cys). The functional group attached can be seen via the inset in each panel. Details of the geometries used can be found in the Supporting Information.

thiol-Michael reaction in a 1:1 mol ratio. The stoichiometry of this reaction is critical because the polymerization/crosslinking during TPL is dictated by the average acrylate functionality of the monomer. The thiol-Michael reaction in this context produces a statistically determined distribution of products depending on the reaction stoichiometry; the average functionality of the monomer mixture determines the extent of crosslinking during TPL. By using a 1:1 molar ratio, we ensured that the final monomer mixture had an average of three acrylates per monomer molecule, which is sufficient for effective crosslinking.[46] ^{1}H and ^{13}C NMR conducted on the products indicated that the thiol-Michael reaction was quantitative within the limit of detection for NMR (details are provided in the Supporting Information). This can be attributed to the following: i) the thiol-Michael reaction is inherently efficient;[47] ii) although the molar ratio of acrylate monomer to thiol was 1:1, the ratio of acrylate to thiol was 4:1. This excess acrylate biases the reaction toward complete consumption of the thiol; iii) the reactions are run without solvent, thus maximizing the concentration of the reactants, which further enhances the reaction conversion. At the end of the reaction, virtually all the thiols are consumed and every acrylate monomer, functionalized or not, necessarily contributes to the statistical average functionality and can participate in the TPL process. Any residual unreacted thiols could potentially increase the shelf life of the monomer by serving as a radical trap, which prevents premature polymerization. During TPL, these residual thiols would be incorporated into the material via thiol–ene chemistry and thus would not adversely affect the polymerization process. The amine catalyst, in addition to being a very minor component of the reaction mixture, is volatile and would have no effect at these concentrations on subsequent TPL or the structures produced

as it is not a photoactive molecule. The fact that these monomers can be used without purification is a key advantage of this approach as it makes this technique broadly accessible to scientists and engineers from a variety of backgrounds.

To demonstrate the versatility of this approach, we synthesized nine different functional acrylates. As a proof of concept, we synthesized monomers that encompassed a wide range of chemical functionalities. The photoresist was then prepared by mixing the functionalized acrylate with 7-diethylamino-3-thenoylcoumarin (DETC), an efficient two-photon photoinitiator,[48] in a small amount of dichloromethane (DCM). The functional resists were then stored under yellow light, displaying no observable change in the TPL performance over a period of three months.

We fabricated a range of structures with different unit cell geometries to highlight the compatibility and versatility of these functional photoresists with the TPL process. For each photoresist, two different structures were made: a lattice comprising multiple small unit cells each ≈20 µm in size and a single large unit cell ≈70 µm tall. Figure 1b–j shows SEM images of fully resolved structures with smooth surfaces, as well as the chemical functionality attached via the thiol-Michael reaction. For all the structures fabricated, the distance between the rastered laser scans in the *x*–*y* plane and the slicing distance of the layers in the *z*-direction were set at a constant 200 nm, the laser power was set at 20 mW, and the writing speed was set at 2 cm s^{-1}. All the structures made were slightly smaller than designed, with shrinkage ranging from 5–13% depending on the photoresist used (more details are given in the Supporting Information). This reduction in size can be attributed to the following: i) the acrylate-based nature of the photoresists used,[49] ii) the use of solvent in preparing the photoresist, and iii) the index of refraction mismatch between the immersion oil, photoresist, and the cross-linked polymer.[35]

To verify that the fabricated structures had the desired functionality, we performed EDS analysis, which allowed us to easily detect the sulfur atoms present in the thioether bond. EDS could also detect elements other than carbon and oxygen on the installed functional groups, i.e., all the monomers described in Figure 1 with the exception of PETTA/OH, PETTA/octane, and PETTA/BM. **Figure 2** depicts the EDS maps of all samples made, with the elemental maps highlighting the presence of sulfur throughout the structure, as well as other distinguishable elements found in the attached functional groups, which provide strong evidence that the fabricated structures exhibit the desired functionality. The clearly visible silhouettes in the EDS elemental maps reveal that the functional groups are homogeneously distributed throughout the samples and are not preferentially localized.

Since most chemical reactions occur on surfaces, it is important to determine if the functional groups of interest are also on the surface. This information cannot be obtained from the EDS maps because the large interaction volume of the electron beam within the polymer makes it impossible to discern whether the signal comes from the surface or from the volume of the sample. Furthermore, surfaces of photoresists can reconstruct during development so it is important to know if any of these functional groups get buried. To more precisely characterize the surface, we performed XPS measurements on 3 mm (L) × 3 mm (W) × 300 nm (H) plates fabricated via TPL (details are provided in the Supporting Information). Figure S1 (Supporting Information) shows the survey spectra of all the plates. The presence of the S 2p peak (≈165 eV) in all the samples is indicative of the thioether bond, which confirms the presence of the functional groups on the surface. This is further supported by the F 1s peak (≈688 eV) in the spectra of PETTA/LCF, PETTA/PFP and PETTA/CH_2CF_3, the N 1s peak (≈400 eV) in PETTA/N-BOC and PETTA/N-BOC(Cys), the Si 2p peak (≈100 eV) in PETTA/SiOMe, and a lack of the S 2p peak in the control PETTA plate. Based on these results, it is reasonable to conclude that the 3D structures also exhibit functionality on the surface because both geometries were identically fabricated via TPL.

Surface functionalization leads to a modification in surface energy. To demonstrate this, we performed contact angle measurements on TPL fabricated plates of PETTA/OH, PETTA/octane, and PETTA/LCF, with PETTA as the control, shown in **Figure 3**. These particular resists were chosen because they theoretically exhibit the widest range of hydrophobicity. Contact angle measurements demonstrate that compared to the control PETTA plate, the PETTA/OH photoresist is more hydrophilic and the PETTA/octane and PETTA/LCF photoresists are more hydrophobic. This observation is expected based on the chemistry of the functional groups: the hydroxyl groups present on the surface of the PETTA/OH plates allow for the formation of hydrogen bonds with water, which makes the surface more hydrophilic. For the PETTA/octane and PETTA/LCF photoresists, the long chain alkanes and fluoroalkanes are nonpolar and do not interact favorably with water, which results in a hydrophobic surface. These results indicate that chemical functionalization provides tunability in surface properties. Considering that nanostructuring of the surface has also been shown to modify its contact angle,[50] the potential combination of nanostructuring and surface chemistry functionalization of the constituent polymer described in this work could be an interesting area for future work, enabling the design of materials with unusual and unprecedented properties.

As mentioned prior, by directly attaching a reactive group to the monomer that is not consumed during the polymerization process, a higher concentration of functional groups can be available for postfunctionalization.[37] The thiol-Michael prefunctionalization approach described here also allows for the fabrication of such reactive structures, which can be used for postfunctionalization reactions. To illustrate this point, we wrote plates of known dimensions using PETTA/N-BOC on glass substrates treated with 3-(trimethoxysilyl)propyl methacrylate to promote adhesion of the polymer.[33] These plates have Boc-protected amines on the surface, which can be easily deprotected in a solution of 50/50 vol% of trifluoroacetic acid (TFA) and DCM, to give primary amines. The number of accessible amines was then quantified using a colorimetric method based on the azo dye Orange II (more details are provided in the Supporting Information).[51–54] Using this method, the surface density of accessible amines was determined to be $3.9 \pm 0.7 \times 10^8$ molecules μm^{-2}, which is significantly higher than that which can be achieved by just using residual unreacted polymerizing groups.[35] Several factors may contribute to such a seemingly high surface density. First, due to the TPL process,

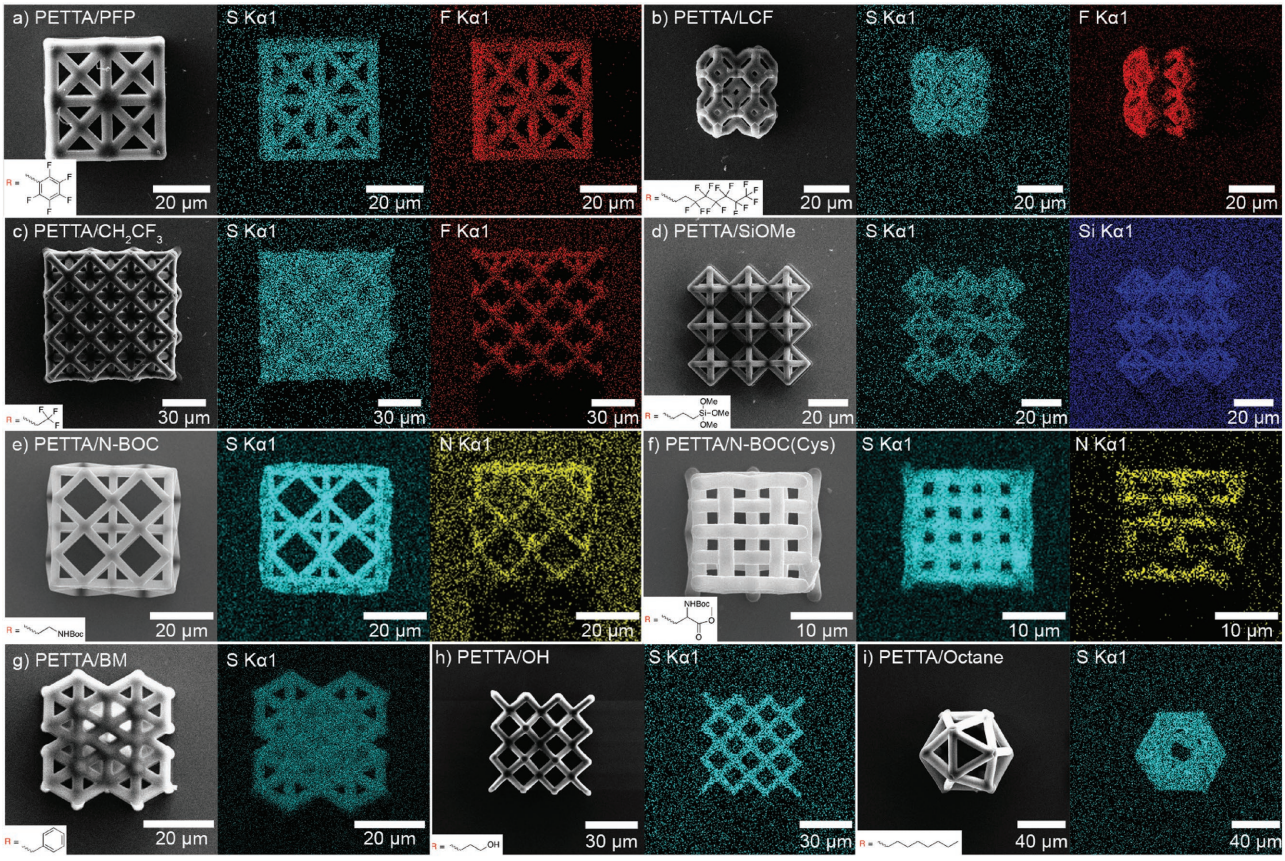

Figure 2. Energy-dispersive X-ray spectroscopy elemental maps for a) PETTA/PFP, b) PETTA/LCF, c) PETTA/CH2CF3, d) PETTA/SiOMe, e) PETTA/N-BOC, f) PETTA/N-BOC(Cys), g) PETTA/BM, h) PETTA/OH, and i) PETTA/Octane. For each set of images, the first image is the SEM image; the second image is the sulfur Kα1 map, and the third image (if applicable) is the distinguishable element map. Insets show the functional group attached.

there is a low degree of monomer conversion on the surface of the structure,[1] leading to some surface swelling, allowing the Orange II molecules access to the amines throughout the swollen surface layer, which might be on the order of tens of nanometers. The dye is able to enter this swollen surface layer of the structure, which means that normalizing the number of amines complexed with the Orange II molecule by the surface area yields the number of accessible amines per unit area of the structure surface. This surface density takes into account the penetration of the dye into the structure and, more importantly, reflects the actual number of surface-accessible amines participating in this reaction. Second, the surface area measurements did not take into account the surface roughness, which would lead to an underestimation of the surface area of the structure. It is important to note that the Orange II test gives a lower bound as to the number of amines that can be complexed with the dye as steric hindrance from bound Orange II molecules potentially limits the accessibility of neighboring amine groups to free Orange II molecules, which would consequently reduce the measured amount of accessible amines.[53]

To visually demonstrate the use of these surface amines for postfunctionalization reactions, we attached a fluorescent molecule via an *N*-hydroxysuccinimide ester (NHS). As a preliminary test, we fabricated 2D structures using TPL and then deprotected the amines in a solution of 50/50 vol% of TFA and DCM, followed by a rinse in aqueous sodium bicarbonate and deionized water. As it is possible for the deprotected amines to react with any unreacted acrylates on the surface, the structures were immediately immersed in a solution containing NHS-fluorescein before being rinsed in dimethylformamide (DMF) and then deionized water. As a control, structures made using PETTA were also subjected to the same procedure. **Figure 4**a–c shows the fluorescence images of the reacted 2D structures and indicates that the fluorescein functional group was successfully attached to the surface of the PETTA/N-BOC and PETTA/N-BOC(Cys) structures evidenced by the strong emission in the detection region of ≈525 nm.

A slight amount of fluorescence was detected in the PETTA control sample because of the auto fluorescence of DETC.[35] To isolate the emission from the fluorescein molecule, we determined the intensity from DETC based on the control sample and subtracted it from that of the PETTA/N-BOC and PETTA/N-BOC(Cys) structures. To more accurately reflect the relative intensity of fluorescence emission, the intensities of all samples in Figure 4a–c were normalized to the maximum intensity detected, i.e., that of PETTA/N-BOC. Normalized fluorescence results show that the emission from the PETTA/N-BOC structure was greater than that of the PETTA/N-BOC(Cys) structure, while virtually no detectable fluorescence emanated from the PETTA control. The reduced relative

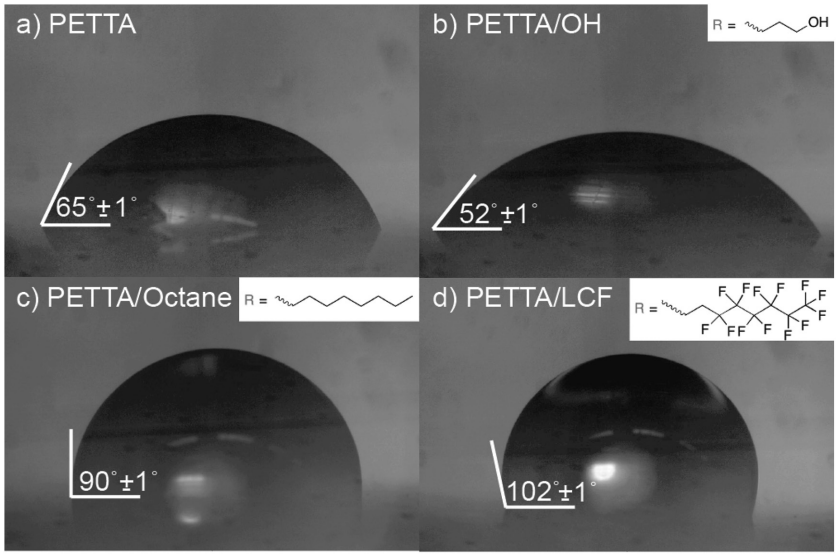

Figure 3. Measurements of the static contact angle of a water droplet on a plate of a) PETTA (control) (65°), b) PETTA/OH (52°), c) PETTA/Octane (90°), and d) PETTA/LCF (102°). All functionalized plates had markedly different contact angles from that of the control, highlighting the effect of functionalization on surface properties. Insets show the functional groups attached.

fluorescence emission from the PETTA/N-BOC(Cys) structures was likely due to a lower reactivity of the amine with the NHS-fluorescein arising from steric hindrance around the primary amine compared with that from PETTA/N-BOC.

We fabricated 3D structures using the same three photoresists and subjected them to the same functionalization procedure. Figure 4d,f shows the normalized fluorescence images of these samples and confirms the successful attachment of the fluorescein molecules to the PETTA/N-BOC and PETTA/N-BOC(Cys) structures and corroborates the findings from the 2D structures. The nonuniform intensities in the 3D fluorescence images arise from capturing all of the emitted light, including that from the unfocused background. To circumvent this, we used confocal fluorescence microscopy to image the 3D structures. Figure 4g,h (more images and videos are given in the Supporting Information) shows uniform intensity, which confirms that the fluorescein was uniformly attached to the structure.

It is worth mentioning that the postfunctionalization methodology described within currently does not allow for spatial control of the reaction. To achieve spatial resolution on the surface of the structures as demonstrated in other works in the literature,[37–39] it is necessary to have photoactive functional groups, which cannot be achieved by using amines alone. However, the approach taken here does not necessarily preclude spatial resolution as photoactive groups could potentially be installed via the amines, which could be subsequently modified on the surface in a spatially controlled manner. The investigation and demonstration of this capability merits its own independent study but is beyond the scope of this report.

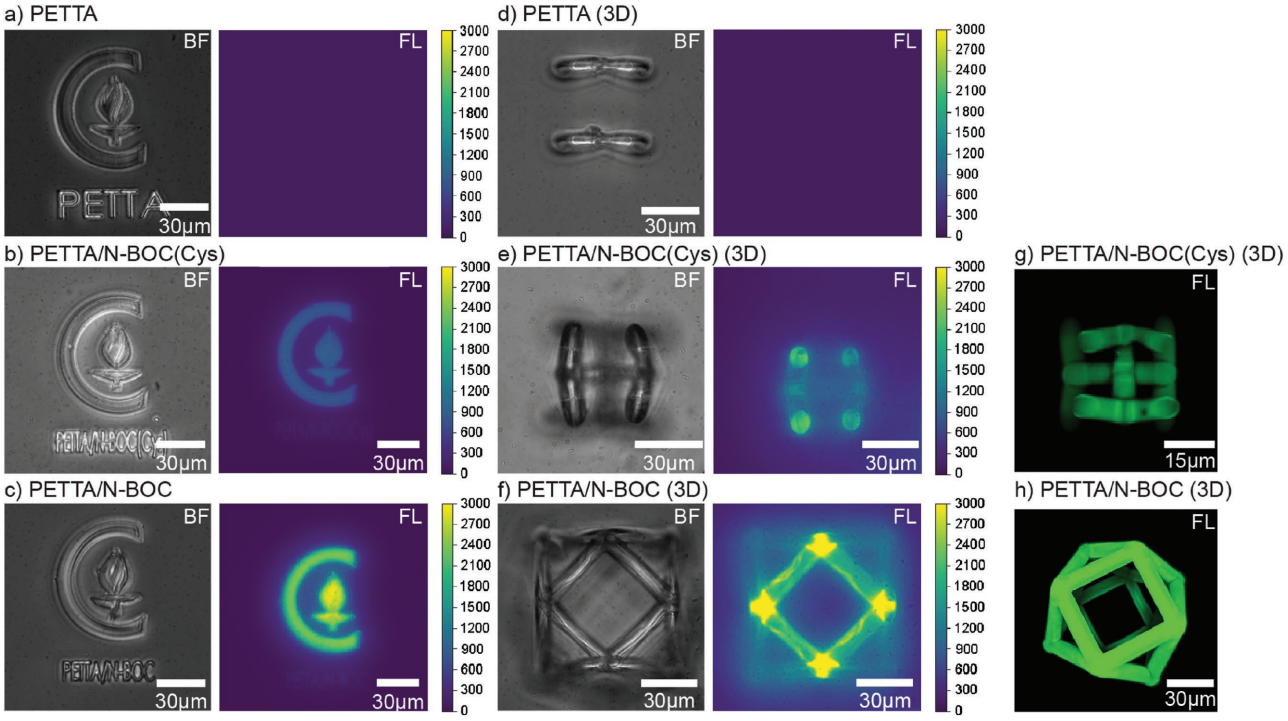

Figure 4. Fluorescence images of 2D structures of a) PETTA, b) PETTA/N-BOC(Cys), and c) PETTA/N-BOC. Fluorescence images of 3D architected materials of d) PETTA, e) PETTA/N-BOC(Cys), and f) PETTA/N-BOC. Each set of images has a bright-field (BF) image and a corresponding fluorescence image (FL). Confocal fluorescence images of g) PETTA/N-BOC(Cys) and h) PETTA/N-BOC.

In conclusion, we fabricated chemically functionalized 3D architected structures by first functionalizing the acrylate monomer via the thiol-Michael reaction and then subsequently polymerizing the functionalized monomer using two-photon lithography. The advantages of this approach are the simplicity of the thiol-Michael reaction and the variety of functional groups that can be attached prepolymerization. EDS maps of all nine fabricated architected structures confirmed the presence of the intended chemical functionality throughout the bulk, and XPS measurements on plates made using the same functional photoresists confirmed their presence on the surface. Contact angle measurements on plates made using PETTA, PETTA/OH, PETTA/octane, and PETTA/LCF showed a marked difference in wetting properties, from hydrophobic (contact angle of 102°) to hydrophilic (contact angle of 52°). We also fabricated reactive structures with functional handles using PETTA/N-BOC and PETTA/N-BOC(Cys). These Boc-protected amines were deprotected to primary amines and reacted with an NHS fluorescein molecule to produce fluorescent structures, as confirmed by fluorescence microscopy. The surface density of accessible primary amines on PETTA/N-BOC plates, as determined by the Orange II test, was $3.9 \pm 0.7 \times 10^8$ molecules μm^{-2}. These functional 3D structures provide an effective pathway for a variety of applications. For example, attaching biologically relevant molecules such as peptides, poly(ethylene glycol) (PEG) chains, or antibodies to the amines could allow for drug delivery or biosensing. The modulation of hydrophobicity based on the functionalization of the monomer enables the fabrication of materials with antifouling properties. The inclusion of the trimethoxysilane group introduces the possibility of performing sol–gel chemistry on the surface of these structures. The diversity of chemical functionality that we have successfully incorporated into these photoresists points to the versatility of this approach. This work conveys a simple, versatile, and effective approach to fabricate 3D structures with virtually any geometry, dimensions, and chemical functionality, which renders it promising for a variety of biomedical, biochemical, and technological applications.

Experimental Section

Materials: All chemicals were acquired from Sigma–Aldrich unless otherwise stated. PETTA, 1-octanethiol (>98.5%), ethanethiol (97%), 3,3,4,4,5,5,6,6,7,7,8,8,8-tridecafluoro-1-octanethiol (97%), 2-mercaptoethanol (>99%), (3-mercaptopropyl) trimethoxysilane (95%), benzyl mercaptan (99%), 2,2,2-trifluoroethanethiol (95%), 2,3,4,5,6-pentafluorothiophenol (97%), 2-(Boc-amino)ethanethiol (97%), *N*-(*tert*-butoxycarbonyl)-L-cysteine methyl ester (97%), hexylamine (99%), TFA (99%), sodium bicarbonate (>99.7%), *N,N*-dimethylformamide (DMF) (>99%), 5(6)-carboxyfluorescein *N*-hydroxysuccinimide ester (NHS fluorescein, >99%, Fisher Scientific), DETC (Exciton), Orange II sodium salt (>85%), 3-(trimethoxysilyl)propyl methacrylate (98%), ethanol (95%, Koptec), hydrochloric acid (36.5–38%, J. T. Baker), acetic acid, glacial (>99.7%, J. T. Baker), sodium hydroxide (>98%, Macron Chemicals), DCM (>99%, Alfa Aesar), propylene glycol monomethyl ether acetate (PGMEA) (>99.5%), and isopropyl alcohol (IPA) (99.7%) were used as received without further purification. Milli-Q quality water (18 MΩ cm) was generated from a Milli-Q reagent water system.

General Procedure for Thiol-Michael Addition Reactions: Pentaerythritol tetraacrylate (1.0 equiv., 3 g, 8.51 mmol), thiol (1.0 equiv., 8.51 mmol), and hexylamine (0.1 equiv., 0.112 mL, 0.85 mmol) were added to a 20 mL scintillation vial. The reaction mixture became warm and homogeneous within 2 min, and was stirred at 40 °C for 14 h. Completion of the reaction was verified by ^{1}H and ^{13}C NMR, and the product was used without any further purification. See the Supporting Information for NMR analysis.

Preparation of Photoresist: DETC (5.6 mg, 1.6 wt%) was first mixed in DCM (20 µL, 8.0 wt%) in a 2.5 mL Eppendorf tube. When the DETC was completely dissolved, the thiol-Michael adduct (0.30 g, 90.4 wt%) was added to the solution. The photoresist was then vortexed for 10 s and stored overnight in ambient yellow light conditions.

Preparation of Functionalized Glass Slide: Glass slides were ultrasonicated in IPA for 15 min and then dried with argon. A 95% ethanol/5% water solution was adjusted to pH 4.5–5.5 with acetic acid. 3-(Trimethoxysilyl)propyl methacrylate was then added to the solution with stirring to yield a 2% final concentration. The cleaned glass slides were then immersed into the silane solution with gentle stirring for 2 min. The slides were then dipped briefly in ethanol to rinse away the excess silane. The silane layer was then cured at 110 °C for 15 min.

^{1}H and ^{13}C NMR Spectroscopy: NMR spectra were taken in deuterated chloroform on a Varian 500 MHz spectrometer. ^{1}H and ^{13}C chemical shifts were referenced relative to $CDCl_3$ ($\delta = 7.26$ for ^{1}H and $\delta = 77.16$ for ^{13}C). ^{19}F chemical shifts were referenced automatically by the VnmrJ software program.

Two-Photon Lithography of 3D Structures: Two-photon lithography was performed using a commercially available system (Photonic Professional GT, Nanoscribe GmbH) using a Zeiss Plan-Apochromat 63×/1.4 Oil DIC objective. Rastering of the laser was achieved via a set of galvo mirrors and piezoelectric actuators. For all structures made, the laser power and scan speed were set at 20 mW and 2 cm s^{-1}, respectively. Glass substrates 30 mm in diameter and 0.17 mm thick were used in conjunction with silicon chips 1 cm (L) × 1 cm (W). The photoresist was drop cast onto the glass substrate and then a silicon chip placed over it, using Kapton tape of ≈100 µm in thickness as a spacer. The structures were then written on the silicon chip via TPL. The finished sample was developed in PGMEA for 30 min followed by an immersion in IPA for 5 min.

Scanning Electron Microscopy: SEM imaging was performed using an FEI Versa 3D DualBeam (FEI co.).

Energy-Dispersive X-Ray Spectroscopy: EDS was conducted using a Zeiss 1550VP FESEM equipped with an Oxford X-Max SDD X-ray energy-dispersive spectrometer (EDS) system. The applied voltage was 15 kV. The samples were coated with a 10 nm carbon layer prior to measurement.

X-Ray Photoelectron Spectroscopy: XPS was performed under 10^{-9} Torr with a Surface Science Instruments M-Probe ESCA controlled by Hawk Data Collection software. The X-ray source was a monochromatic Al K_α line at 1486.6 eV. All spectra were collected using a spot size of 800 µm. A low-energy electron flood gun was used to minimize charging effects. Survey scans from 0 to 1000 eV using a pass energy of 150 eV and a step size of 1 eV were performed to identify the elements that were present on the surface. The XPS data were analyzed using CasaXPS 2.3.17.

Contact Angle Measurements: The contact angle data were obtained using a contact angle goniometer equipped with an AmScope Microscope Camera model MU300. A syringe was used to place a water droplet on the surface of the polymer plates. The image was captured 10 s after the drop was placed and then analyzed using ImageJ and DropSnake (software developed at Ecole Polytechnique Federale De Lausanne). Each reported contact angle was the average of four different measurements.

Orange II Amine Test: Adapted from Noel et al.[53] plates of PETTA/N-BOC were written on the functionalized glass slides using TPL. The plates were deprotected in a solution of TFA and DCM (50/50 vol%) for 60 min. The Orange II dye solution was prepared using Milli-Q water adjusted to pH 3 using hydrochloric acid. The plates were then immersed in a 7 mL Orange II acidic solution (14 mg mL^{-1}) for 30 min at 40 °C. The plates were then rinsed five times using the pH 3 solution to remove excess dye and then dried with argon. The colored plates

were then immersed in a known volume of alkaline solution at 40 °C (Milli-Q water adjusted to pH 12 with a 1 M NaOH solution). When the plates were no longer colored, they were removed from the solution and the pH of the solution was adjusted to pH 3 by adding concentrated hydrochloric acid. The absorbance of the solution containing the desorbed dye was then measured at 480 nm. The measured absorbance was then correlated to the concentration of Orange II in solution via the use of a calibration curve.

Fluorescence-Tagging Experiments: The PETTA/N-BOC and PETTA/N-BOC(Cys) samples were written on the functionalized glass slides using TPL. The fabricated samples were first deprotected by soaking them in a solution of TFA and DCM (50/50 vol%) for 15 min. The samples were then soaked in an excess aqueous solution of sodium bicarbonate, followed by excess deionized water. To prepare the fluorescence molecule, 10 mg of NHS fluorescein was dissolved in 3 mL of DMF. The sample was then immersed in the solution of NHS fluorescein/DMF solution, which was then left in the dark for 60 min. To remove the unreacted NHS fluorescein, the samples were soaked in DMF for 15 min and then for another 15 min in deionized water. The samples were then dried using an air gun and then stored in the dark.

Fluorescence Microscopy: The fluorescence images were obtained using a Nikon Eclipse Ti-E and the software Micro-Manager (developed by the University of California, San Francisco). The objective lens used was a 40× air objective. Bright field images were imaged in transmission mode. Fluorescence images were imaged using a broad-spectrum mercury lamp with an excitation filter between 457 and 487 nm and a fluorescence emission filter between 502 and 538 nm. All the samples were excited for 5 ms each.

Confocal Fluorescence Microscopy: Fluorescein-labeled structures were visualized using a confocal laser scanning microscope Zeiss model LSM 800 equipped with a 20× water immersion objective (Achroplan, NA = 0.5). The structures were directly mounted in the objective immersion water. A 488 nm laser line was used for excitation and the emission was measured between 500 and 550 nm. We acquired *z*-stacks with 1 µm spacing between successive slices. Imaris (developed by Bitplane) was used to generate 3D visualization and movies of our structures.

Supporting Information

Supporting Information is available from the Wiley Online Library or from the author.

Acknowledgements

D.W.Y. and M.D.S. contributed equally to this work. This study was supported by a grant from the National Institutes of Health (Grant No. 1R01CA194533). The authors acknowledge support from the Molecular Materials Research Center of the Beckman Institute at the California Institute of Technology. Imaging was performed in the Biological Imaging Facility, with the support of the Caltech Beckman Institute and the Arnold and Mabel Beckman Foundation. The authors also acknowledge Mr. Soichi Hirokawa for performing the fluorescence microscopy, Dr. Alexandre Persat for his help with the confocal microscopy, Dr. Zachary Sternberger for image processing assistance, Dr. Lucas Meza for two-photon lithography support, and Dr. Stéphane Delalande for discussions concerning polymer synthesis. The authors declare no competing financial interest.

Received: September 30, 2016
Revised: December 22, 2016
Published online: February 20, 2017

[1] T. Baldacchini, *Three-Dimensional Microfabrication Using Two-Photon Polymerization: Fundamentals, Technology, and Applications*, William Andrew, Waltham, MA, USA **2015**.
[2] C. N. LaFratta, J. T. Fourkas, T. Baldacchini, R. A. Farrer, *Angew. Chem., Int. Ed.* **2007**, *46*, 6238.
[3] K. Lee, R. H. Kim, D. Yang, S. H. Park, *Prog. Polym. Sci.* **2008**, *33*, 631.
[4] L. Li, J. T. Fourkas, *Mater. Today* **2007**, *10*, 30.
[5] M. Malinauskas, M. Farsari, A. Piskarskas, S. Juodkazis, *Phys. Rep.* **2013**, *533*, 1.
[6] H. Sun, S. Kawata, in *NMR · 3D Analysis · Photopolymerization; Advances in Polymer Science, Vol. 170*, Springer, Berlin, Germany **2004**, pp. 169–273.
[7] S. Maruo, O. Nakamura, S. Kawata, *Opt. Lett.* **1997**, *22*, 132.
[8] S. Wu, J. Serbin, M. Gu, *J. Photochem. Photobiol, A* **2006**, *181*, 1.
[9] A. Selimis, V. Mironov, M. Farsari, *Microelectron. Eng.* **2015**, *132*, 83.
[10] T. Y. Huang, M. S. Sakar, A. Mao, A. J. Petruska, F. Qiu, X. B. Chen, S. Kennedy, D. Mooney, B. J. Nelson, *Adv. Mater.* **2015**, *27*, 6644.
[11] C. Peters, M. Hoop, S. Pané, B. J. Nelson, C. Hierold, *Adv. Mater.* **2016**, *28*, 533.
[12] A. Otuka, D. Corrêa, C. R. Fontana, C. Mendonça, *Mater. Sci. Eng. C* **2014**, *35*, 185.
[13] P. Danilevicius, S. Rekstyte, E. Balciunas, A. Kraniauskas, R. Jarasiene, R. Sirmenis, D. Baltriukiene, V. Bukelskiene, R. Gadonas, M. Malinauskas, *J. Biomed. Opt.* **2012**, *17*, 0814051.
[14] J. Torgersen, A. Ovsianikov, V. Mironov, N. Pucher, X. Qin, Z. Li, K. Cicha, T. Machacek, R. Liska, V. Jantsch, *J. Biomed. Opt.* **2012**, *17*, 105008.
[15] M. T. Raimondi, S. M. Eaton, M. M. Nava, M. Laganà, G. Cerullo, R. Osellame, *J. Appl. Biomater. Funct. Mater.* **2012**, *10*, 55.
[16] T. Gissibl, S. Thiele, A. Herkommer, H. Giessen, *Nat. Photonics* **2016**, *10*, 554.
[17] A. Žukauskas, M. Malinauskas, C. Reinhardt, B. N. Chichkov, R. Gadonas, *Appl. Opt.* **2012**, *51*, 4995.
[18] V. Chernow, H. Alaeian, J. Dionne, J. R. Greer, *Appl. Phys. Lett.* **2015**, *107*, 101905.
[19] J. K. Gansel, M. Thiel, M. S. Rill, M. Decker, K. Bade, V. Saile, G. von Freymann, S. Linden, M. Wegener, *Science* **2009**, *325*, 1513.
[20] H. Xia, J. Wang, Y. Tian, Q. D. Chen, X. B. Du, Y. L. Zhang, Y. He, H. B. Sun, *Adv. Mater.* **2010**, *22*, 3204.
[21] C. Peters, O. Ergeneman, P. D. W. García, M. Müller, S. Pané, B. J. Nelson, C. Hierold, *Adv. Funct. Mater.* **2014**, *24*, 5269.
[22] J. Wang, H. Xia, B. Xu, L. Niu, D. Wu, Q. Chen, H. Sun, *Opt. Lett.* **2009**, *34*, 581.
[23] R. Krini, C. W. Ha, P. Prabhakaran, H. E. Mard, D. Y. Yang, R. Zentel, K. S. Lee, *Macromol. Rapid Commun.* **2015**, *36*, 1108.
[24] Z. B. Sun, X. Z. Dong, W. Q. Chen, S. Nakanishi, X. M. Duan, S. Kawata, *Adv. Mater.* **2008**, *20*, 914.
[25] A. Wickberg, J. B. Mueller, Y. J. Mange, J. Fischer, T. Nann, M. Wegener, *Appl. Phys. Lett.* **2015**, *106*, 133103.
[26] Y. Liu, W. Xiong, L. Jiang, Y. Zhou, Y. Lu, *Proc. SPIE* **2016**, *9738*, 973808, DOI:10.1117/12.2214862.
[27] M. Mizoshiri, S. Arakane, J. Sakurai, S. Hata, *Appl. Phys. Exp.* **2016**, *9*, 036701.
[28] S. Ushiba, S. Shoji, K. Masui, J. Kono, S. Kawata, *Adv. Mater.* **2014**, *26*, 5653.
[29] J. J. Park, X. Bulliard, J. M. Lee, J. Hur, K. Im, J. M. Kim, P. Prabhakaran, N. Cho, K. S. Lee, S. Y. Min, *Adv. Funct. Mater.* **2010**, *20*, 2296.
[30] E. Blasco, J. Müller, P. Müller, V. Trouillet, M. Schön, T. Scherer, C. Barner-Kowollik, M. Wegener, *Adv. Mater.* **2016**, *28*, 3592.
[31] Y. Chen, A. Tal, S. M. Kuebler, *Chem. Mater.* **2007**, *19*, 3858.
[32] B. L. Aekbote, J. Jacak, G. J. Schütz, E. Csányi, Z. Szegletes, P. Ormos, L. Kelemen, *Eur. Polym. J.* **2012**, *48*, 1745.
[33] R. A. Farrer, C. N. LaFratta, L. Li, J. Praino, M. J. Naughton, B. E. Saleh, M. C. Teich, J. T. Fourkas, *J. Am. Chem. Soc.* **2006**, *128*, 1796.

[34] M. S. Hahn, J. S. Miller, J. L. West, *Adv. Mater.* **2006**, *18*, 2679.
[35] A. S. Quick, J. Fischer, B. Richter, T. Pauloehrl, V. Trouillet, M. Wegener, C. Barner-Kowollik, *Macromol. Rapid Commun.* **2013**, *34*, 335.
[36] A. S. Quick, A. de los Santos Pereira, M. Bruns, T. Bückmann, C. Rodriguez-Emmenegger, M. Wegener, C. Barner-Kowollik, *Adv. Funct. Mater.* **2015**, *25*, 3735.
[37] T. K. Claus, B. Richter, V. Hahn, A. Welle, S. Kayser, M. Wegener, M. Bastmeyer, G. Delaittre, C. Barner-Kowollik, *Angew. Chem., Int. Ed.* **2016**, *55*, 3817.
[38] B. Richter, T. Pauloehrl, J. Kaschke, D. Fichtner, J. Fischer, A. M. Greiner, D. Wedlich, M. Wegener, G. Delaittre, C. Barner-Kowollik, *Adv. Mater.* **2013**, *25*, 6117.
[39] A. Ovsianikov, Z. Li, J. Torgersen, J. Stampfl, R. Liska, *Adv. Funct. Mater.* **2012**, *22*, 3429.
[40] L. P. C. Gomez, A. Spangenberg, X. A. Ton, Y. Fuchs, F. Bokeloh, J. P. Malval, B. Tse Sum Bui, D. Thuau, C. Ayela, K. Haupt, *Adv. Mater.* **2016**, *28*, 5931.
[41] C. De Marco, A. Gaidukeviciute, R. Kiyan, S. M. Eaton, M. Levi, R. Osellame, B. N. Chichkov, S. Turri, *Langmuir* **2012**, *29*, 426.
[42] A. M. Kloxin, A. M. Kasko, C. N. Salinas, K. S. Anseth, *Science* **2009**, *324*, 59.
[43] O. Kufelt, A. El-Tamer, C. Sehring, S. Schlie-Wolter, B. N. Chichkov, *Biomacromolecules* **2014**, *15*, 650.
[44] A. Ovsianikov, A. Deiwick, S. Van Vlierberghe, M. Pflaum, M. Wilhelmi, P. Dubruel, B. Chichkov, *Materials* **2011**, *4*, 288.
[45] A. I. Ciuciu, P. J. Cywiński, *RSC Adv.* **2014**, *4*, 45504.
[46] G. Odian, *Principles of Polymerization*, John Wiley & Sons, Hoboken, NJ, USA **2004**.
[47] D. P. Nair, M. Podgórski, S. Chatani, T. Gong, W. Xi, C. R. Fenoli, C. N. Bowman, *Chem. Mater.* **2013**, *26*, 724.
[48] J. Fischer, J. B. Mueller, J. Kaschke, T. J. Wolf, A. Unterreiner, M. Wegener, *Opt. Express* **2013**, *21*, 26244.
[49] C. Schmidt, T. Scherzer, *J. Polym. Sci., Part B: Polym. Phys.* **2015**, *53*, 729.
[50] W. Zhang, Z. Yu, Z. Chen, M. Li, *Mater. Lett.* **2012**, *67*, 327.
[51] E. Uchida, Y. Uyama, Y. Ikada, *Langmuir* **1993**, *9*, 1121.
[52] W. Albrecht, B. Seifert, T. Weigel, M. Schossig, A. Holländer, T. Groth, R. Hilke, *Macromol. Chem. Phys.* **2003**, *204*, 510.
[53] S. Noel, B. Liberelle, L. Robitaille, G. De Crescenzo, *Bioconjugate Chem.* **2011**, *22*, 1690.
[54] B. Seifert, G. Mihanetzis, T. Groth, W. Albrecht, K. Richau, Y. Missirlis, G. Von Sengbusch, *Artif. Organs* **2002**, *26*, 189.